Imaging Flux Vortices in MgB_2 using Transmission Electron Microscopy — Supplementary Information

J.C. Loudon,* C.J. Bowell,† and P.A. Midgley

Department of Materials Science and Metallurgy, University of Cambridge, Pembroke Street, Cambridge CB2 3QZ, United Kingdom

N.D. Zhigadlo and J. Karpinski

Laboratory for Solid State Physics, ETH Zurich, Schafmattstrasse 16, CH-8093, Zurich, Switzerland

(Dated: November 29, 2011)

SUPPLEMENTARY INFORMATION 1:
DETAILED EXPERIMENTAL METHODS

MgB_2 single crystals were synthesised by Dr J. Karpinski via the peritectic decomposition of $MgNB_9$ as described in ref. [1]. The samples were thinned to 250 nm in the *c*-direction so that they were electron transparent. Cleaving MgB_2 appears to be very difficult as Uchiyama *et al.* [2] report that as of 2003, they were the only group to successfully cleave MgB_2 for angle-resolved photoemission specroscopy which requires only one cleave whereas sample preparation for electron microscopy involves cleaving the sample many times until electron-transparency is achieved. We had no success in cleaving MgB_2 using sticky-tape as we had done with $Bi_2Sr_2CaCu_2O_{8-\delta}$ [3] and instead we thinned a 30×15 µm area of MgB_2 by focussed ion-beam milling using a dual-beam focussed ion-beam microscope (FIB– the Helios Nanolab) equipped with a micromanipulator. We first tried using the 'lift-out' technique to produce a free-standing thin film of MgB_2 attached to a pillar on a copper grid. These samples proved incredibly fragile, however (being about 3 times the size of a standard sample), and so the standard 'H-bar' geometry was used instead where the thin window is cut into the bulk sample so that it is supported on three sides. The sample needs to be tilted to a high angle (α in Fig. 1(a)) and our specimen stage only allowed tilting to 25° so the specimen was mounted on a pillar, tilted to 45° as illustrated in Fig. 1(b). The tilting angle used in the experiment could be determined to the nearest degree as the tilting angle required to view the thin region edge-on measured in the FIB was $55 \pm 1°$. The sample was in shadow at this orientation when inserted into the transmission electron microscope and required tilting back by 10° giving a tilt angle $\alpha = 45 \pm 1°$.

Micrscopy was undertaken using a Philips CM300 transmission electron microscope operated at 300 kV and equipped with a electron biprism for holography, a 'Lorentz' lens and a Gatan imaging filter. Energy-filtered images were recorded with a 20 eV energy window. The microscope was operated in low-magnification mode at a nominal magnification of 105× with the main objective lens turned off (which can be done by turning the diffraction-focus to its minimum setting) and focussing the image with the diffraction lens. This proved more convenient than using 'Lorentz mode' as a wider range of defoci could be accessed and electron holograms could be acquired with a much larger field of view (4.5 µm with 11% holographic fringe contrast instead of ∼1 µm in Lorentz mode). A magnetic field was

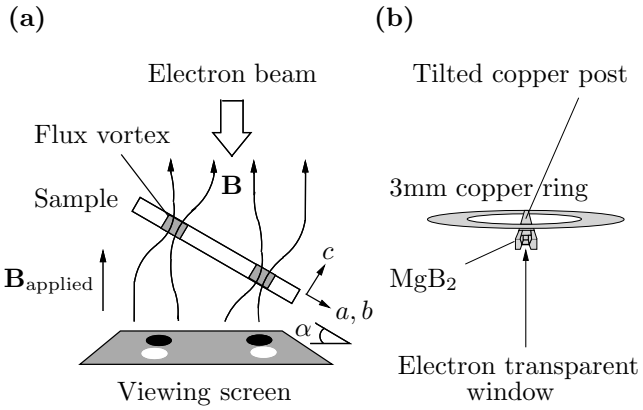

FIG. 1. (a) Experimental arrangement for imaging flux vortices. The electrons are deflected by the component of the B-field from the vortices normal to the electron beam giving a black-white feature in an out-of-focus image. (b) The specimen geometry. The MgB_2 specimen was mounted to a copper post glued to a standard 3 mm diameter copper ring at an angle of 45°. An electron transparent window was then cut by focussed ion-beam milling.

applied to the sample by altering the strength of the twin lens (which can be done in the 'column-align' menu). Low-magnification mode also has the property that the selected area apertures become objective apertures and *vice versa* which is useful for Foucault imaging and taking diffraction patterns (not done for this experiment) whereas in Lorentz mode neither set of apertures is in the image or diffraction planes. The sample was cooled to liquid helium temperatures using a Gatan liquid-helium cooled 'IKHCHDT3010-Special' tilt-rotate holder which has a base temperature of 10 K.

The defocus was calibrated by taking images of Agar Scientific's 'S106' calibration specimen with the same lens settings as the original images. The specimen consists of a cross grating of lines with 2160 lines/mm ruled on an amorphous carbon specimen and the power spectrum of these images consists of a series of rings corresponding to the contrast transfer function of the microscope as well as spots corresponding to the repetition of the grating. This allowed an absolute measurement of the radii of the rings in reciprocal space from which the defocus, Δf, can be calculated as the intensity of the rings is proportional to $\sin^2(\pi \Delta f \lambda_e k^2)$ (where λ_e is the electron wavelength and k the reciprocal space coordinate). (Note that the effect of spherical aberration is negligible under these conditions.)

A thickness map of the specimen was created by dividing an unfiltered image by an energy-filtered image and taking the natural logarithm [4] to create a 't/λ' map which gives

the thickness, t, as a multiple of the inelastic mean free path, λ. To determine λ, an electron hologram was taken at room temperature at an edge of the specimen which gives a phase shift, $\phi = C_E V_0 t$. C_E is a constant which depnds only on the microscope voltage and has the value 6.523×10^6 $\mathrm{m^{-1}V^{-1}}$ at 300 kV. V_0, the mean inner potential, was calculated from theoretical scattering factors given in ref. [5] which gave $V_0 = 17.71$ V. This gave $\lambda = 152 \pm 2$ nm. (Ideally the thickness of the whole specimen would have been determined by electron holography but the field of view afforded by holography was not large enough.)

SUPPLEMENTARY INFORMATION 2: ORIGINAL IMAGES

Fig. 2 shows the images of flux vortices in MgB_2 as they were originally acquired.

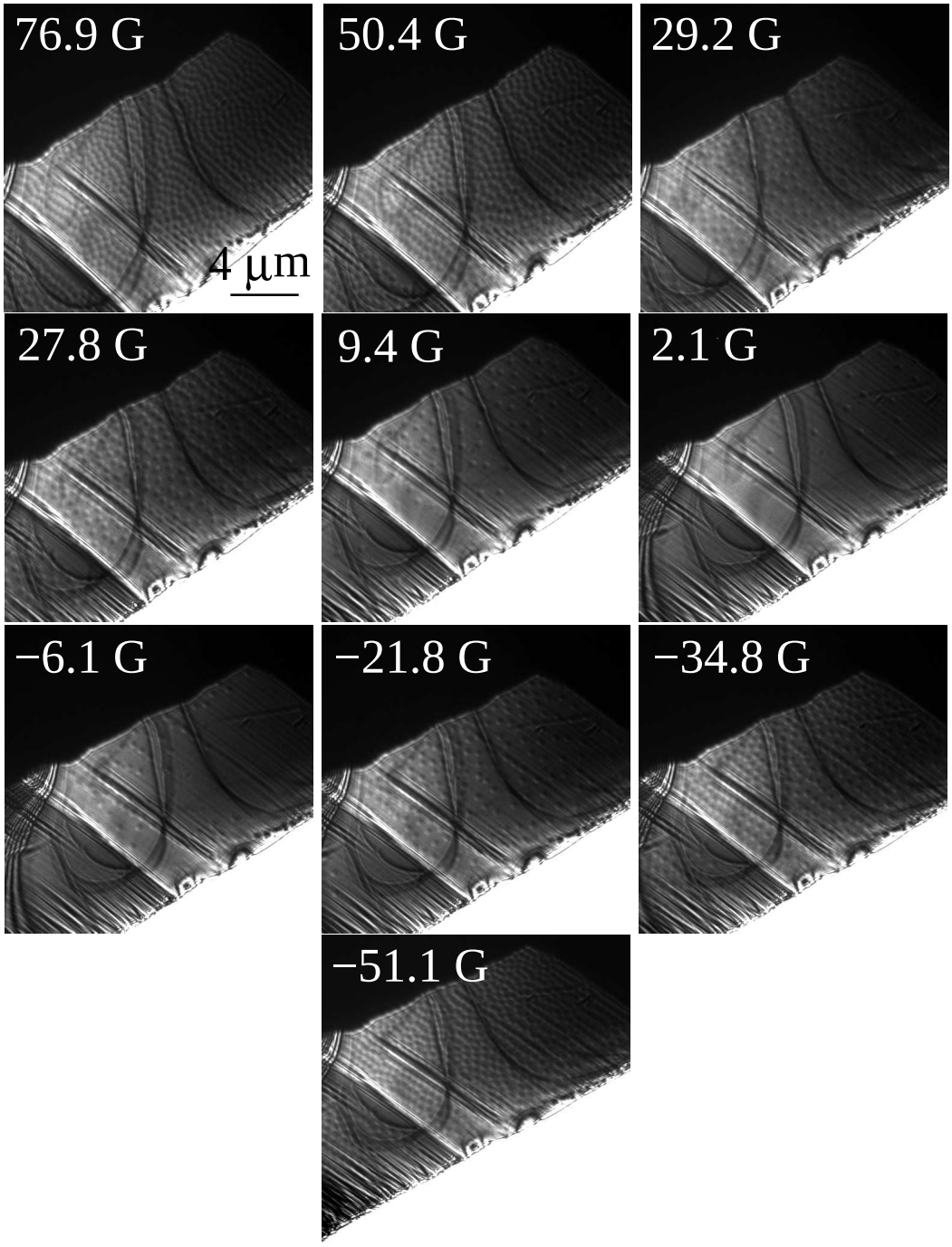

FIG. 2. Original images showing flux vortices in MgB_2 taken at 10.8 K with a defocus of 3.46 ± 0.02 cm at different B-fields (indicated on the images).

SUPPLEMENTARY INFORMATION 3:
ESTIMATION OF THE ENERGIES WHICH DETERMINE THE VORTEX-LATTICE STRUCTURE

The arrangement the flux vortices adopt is due to an energy balance between the repulsive interaction between the vortices (which encourages the formation of a hexagonal lattice) and the energy cost involved in changing the length of a flux vortex due to the specimen not having a uniform thickness. We can estimate these energies as follows:

The energy required to lengthen a flux vortex is directly proportional to its length and depends on the penetration depth, Λ, and coherence length, ξ. The energy per unit length is given by [6]

$$u = \frac{\Phi_0^2}{4\mu_0\pi\Lambda^2}\ln\left(\frac{\Lambda}{\xi}\right).$$

A wide range of values for Λ and ξ have been given in the literature as summarised in ref. [7]. Table I shows some of the values for the penetration depth and coherence length in MgB_2 and values in the final row (calculated for the *ab*-plane) show that it requires and energy of ~ 0.5 eV to lengthen a flux vortex by 1 nm.

We now compare this with the energy cost of moving a flux vortex a distance R away from its equilibrium position in an ideal hexagonal lattice with an average vortex spacing of r. For the vortex arrangements studied here, $r \gg \Lambda$ and so the dominant contribution to the repulsive energy is from the monopoles of strength $\pm\Phi_0$ at the top and bottom surfaces of

TABLE I. Values for the penetration depth and coherence length for MgB_2. Note: Manzano *et al.* give two sets of values for the penetration depth as their calculation is dependent on the value of the anisotropy $\gamma \equiv \Lambda_c/\Lambda_{ab}$ over which there is some disagreement.

	Moschalkov *et al.* [8]	Cubitt *et al.* [9]	Manzano *et al.* [10]
ξ_{ab}/nm	13	8 ± 1	5.5
ξ_c/nm	51		
Λ_{ab}/nm	47.8	82 ± 2	130 or 110
Λ_c/nm	33.6		210 or 280
u/eV nm^{-1}	0.96	0.59 ± 0.03	0.32 or 0.42

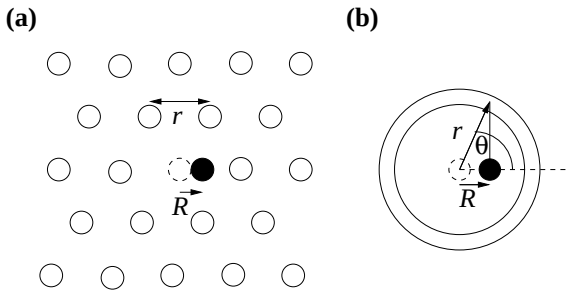

FIG. 3. (a) An ideal hexagonal lattice of flux vortices with average spacing r with one vortex (in black) displaced from its equilibrium position by R. (b) To calculate the energy of this displacement, the neighbouring vortices are approximated to a ring with 'charge' $6\Phi_0$ of radius r.

the specimen where the vortex ends. The repulsive energy between two vortices a distance r apart (also calculated in ref. [11]) is thus

$$U = \frac{\Phi_0^2}{\pi\mu_0 r}$$

In Fig. 3(a), an ideal hexagonal lattice of vortices with average spacing r is shown with the vortex in the middle displaced from its ideal position by R. We wish to calculate the energy associated with such a displacement. If we consider only the nearest neighbours surrounding the displaced vortex and further approximate the surrounding vortices to a ring with 'charge' $6\Phi_0$ as shown in Fig. 3(b), we find that if the displacement, $R = 0$, the energy is

$$U_0 = \frac{6\Phi_0^2}{\pi\mu_0 r}$$

whereas for a non-zero displacement the energy is

$$U_R = \int_0^{2\pi} \frac{6\Phi_0^2/2\pi}{\pi\mu_0\sqrt{r^2 + R^2 - 2rR\cos\theta}}\,\mathrm{d}\,\theta.$$

If the displacement from equilibrium $R \ll r$, we can Taylor approximate this to

$$U_R \approx \frac{3\Phi_0^2}{\pi^2\mu_0 r}\int_0^{2\pi}\left(1 - \frac{R^2}{2r^2} + \frac{3}{2}\frac{R^2}{r^2}\cos^2\theta\right)\,\mathrm{d}\,\theta$$

After performing the integral, it can be seen that the energy cost of moving a vortex from is equilibrium position by a distance R in a lattice of average spacing r is

$$\Delta U \equiv U_R - U_0 = \frac{3\Phi_0^2}{2\pi\mu_0}\frac{R^2}{r^3} = 10140R^2/r^3 \text{ eV (for } r \text{ and } R \text{ in nm)}$$

At the heighest B-field applied in this experiment, 51 G, the average vortex spacing was 617 nm with a standard deviation of 135 nm. Using these as values for r and R respectively gives $U = 0.80$ eV. For the lowest field (2.06 G) the average spacing is 2340 nm and the standard deviation is 760 nm giving $U = 0.44$ eV and it can be seen that these energies are comparable with the energy required for the vortex to climb onto a thickness undulation. In contrast, the thermal energy at 10.8 K at which the images were taken is $k_B T = 0.0009$ eV.

SUPPLEMENTARY INFORMATION 4: IMAGES WITH HISTOGRAMS

An alternative method to using autocorrelation functions (see main paper) to assess the vortex order is to use Delaunay triangulation to create 'bonds' connecting each vortex to its nearest neighbours and plotting histograms to show the distribution of vortex spacings (bond lengths) and bond directions as shown in Fig. 4.

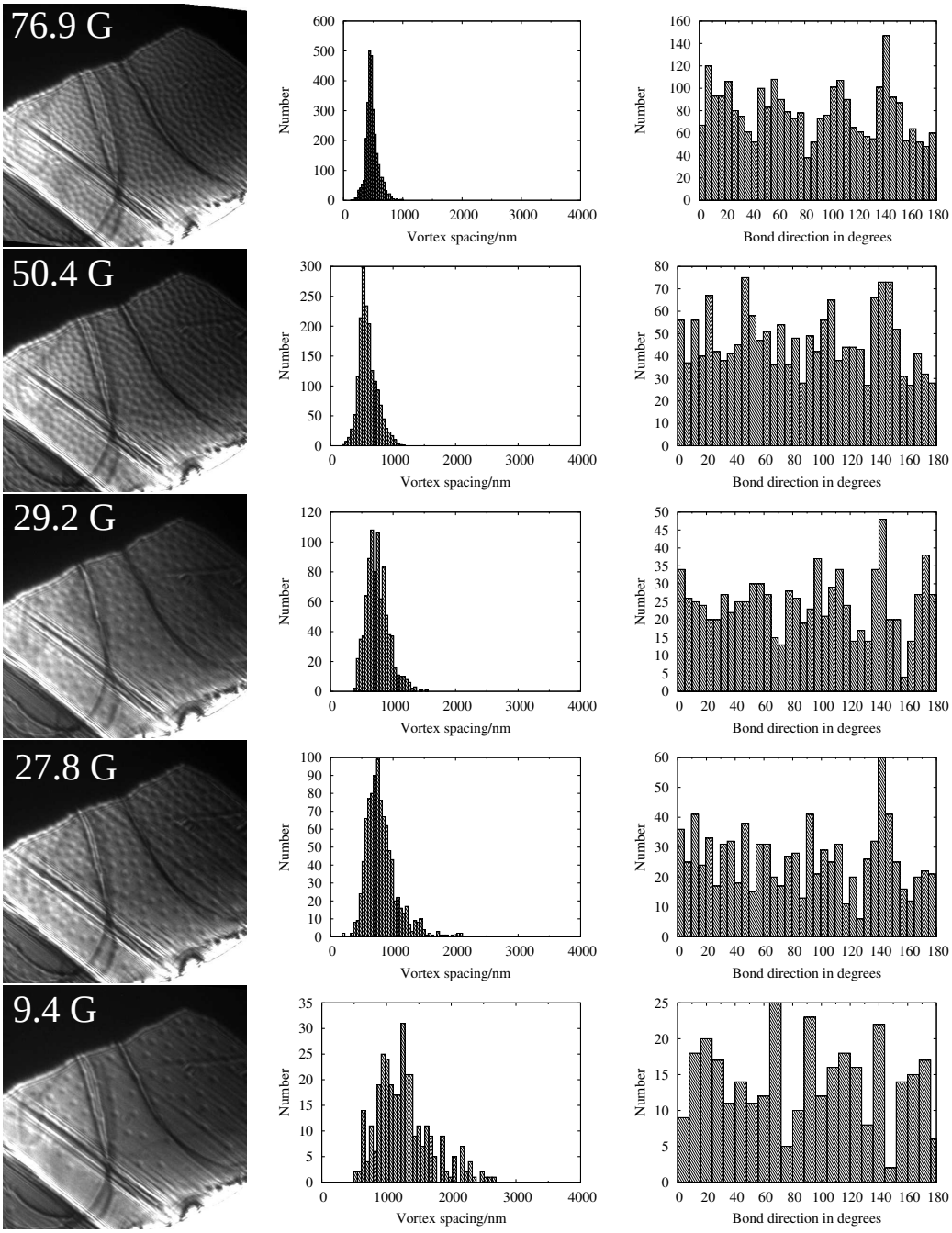

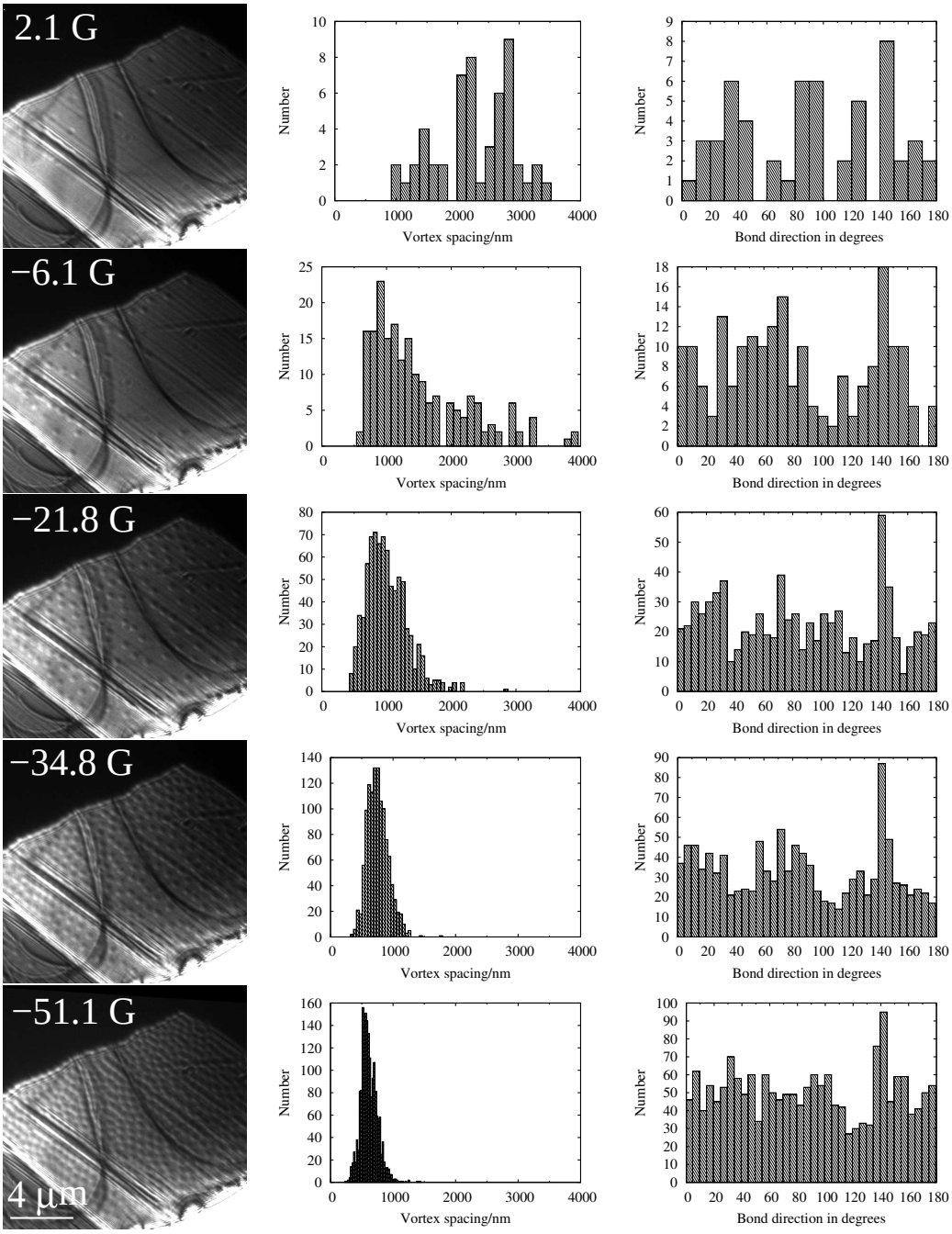

FIG. 4. Sequence of tilt-compensated images showing flux vortices in MgB_2 taken at 10.8 K with a defocus of 3.46 ± 0.02 cm at different B-fields (indicated on the images). Delaunay triangulation was used to create 'bonds' connecting each vortex to its nearest neighbours and the histograms beside each image show the distribution of vortex spacings (bond lengths) and the distribution of bond directions with angles measured anticlockwise from the borizontal.

SUPPLEMENTARY INFORMATION 5:
CIRCUMFERENTIAL LINESCAN OF THE AUTOCORRELATION FUNCTION

Weak maxima can be seen in the inner ring of the autocorrelation function of the vortex positions at 76.9 G as shown in the circumferential linescan in Fig. 5(c). The function is periodic every 180° and peaks occur at 10, 55, 107 and 143°. The angular separation between peaks is 45, 52, 36 and 47°. The fact that the angular separations are closer to 45° than to 60° and that there are 4 peaks in 180° indicates that there is a tendency towards a square lattice of vortices rather than a hexagonal lattice and that two different grains are present, each oriented at approximately 45° to one another. The same conclusion can be drawn from the 4-peaked structure of the histogram for the bond directions at 76.9 G in Fig 4.

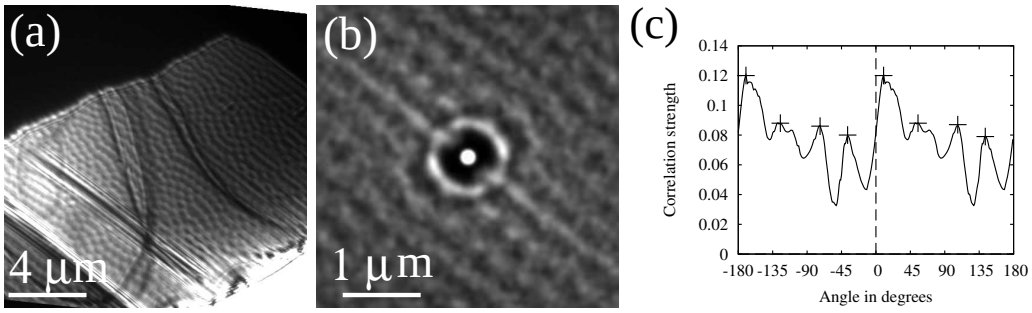

FIG. 5. (a) Tilt-compensated image showing flux vortices in MgB_2 in a field of 76.9 G. (b) The autocorrelation function of the vortex positions. (c) A circumferential linescan of the inner ring of the autocorrelation function with positive angles measured anticlockwise from the horizontal. The peaks in the linescan are marked with crosses and occur at -125, -73, -37, 10, 55, 107 and 143°. The autocorrelation function is plotted so that a perfect correlation gives a value of 1, perfect anticorrelation -1 and no correlation is given 0 as explained in ref. [3].

* j.c.loudon@gmail.com

† Now at Halcyon Molecular, 505 Penobscot Drive, Redwood City, CA 94063, USA.

[1] J. Karpinski, S. M. Kazakov, J. Jun, M. Angst, R. Puzniak, A. Wisniewski, and P. Bordet, Physica C **385**, 42 (2003).

[2] H. Uchiyama, S. Tajima, K. M. Shen, D. H. Lu, and Z. X. Shen, Physica C **385**, 85 (2003).

[3] J. C. Loudon and P. A. Midgley, Ultramicroscopy **109**, 700 (2009).

[4] R. F. Egerton, Rep. Prog. Phys. **72**, 1 (2009).

[5] D. Rez, P. Rez, and I. Grant, Acta. Cryst. **A50**, 481 (1994).

[6] J. F. Annett, *Superconductivity, Superfluids and Condensates* (Oxford University Press, Oxford, 2004).

[7] A. A. Golubov, A. Brinkman, O. Dolgov, J. Kortus, and O.Jespen, Phys. Rev. B. **66**, 054524 (2002).

[8] V. Moshchalkov, M. Menghini, T. Nishio, Q. H. Chen, A. V. Silhanek, V. H. Dao, L. Chibotaru, N. Zhigadlo, and J. Karpinski, Phys. Rev. Lett. **102**, 117001 (2009).

[9] R. Cubitt, M. R. Eskildsen, C. D. Dewhurst, J. Jun, S. M. Kazakov, and J. Karpinski, Phys. Rev. Lett. **91**, 047002 (2003).

[10] F. Manzano, A. Carrington, N. E. Hussey, S. Lee, A. Yamamoto, and S. Tajima, Phys. Rev. Lett. **88**, 047002 (2002).

[11] J. R. Clem, Phys. Rev. B. **43**, 7837 (1991).